Please cite the Published Version

Additional Information: This is an open access article which first appeared in Journal of Hydrology

Data Access Statement: Data will be made available on request.
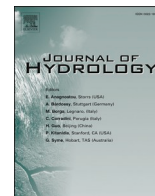
Research papers

Drainage ditch network extraction from lidar data using deep convolutional neural networks in a low relief landscape

Ling Du [a,b], Gregory W. McCarty [b,*], Xia Li [c,*], Xin Zhang [d], Martin C. Rabenhorst [a], Megan W. Lang [e], Zhenhua Zou [f], Xuesong Zhang [b], Audra L. Hinson [b]

[a] Department of Environmental Science & Technology, University of Maryland, College Park, MD 20742, USA
[b] Hydrology and Remote Sensing Laboratory, USDA-ARS, Beltsville, MD 20705, USA
[c] Research and Development Center for Watershed Environmental Eco-Engineering, Beijing Normal University, Zhuhai, Guangdong, 519087, China
[d] Department of Computing and Mathematics, Manchester Metropolitan University, Manchester M1 5GD UK
[e] U.S. Fish and Wildlife Service National Wetlands Inventory, Falls Church, VA 22041, USA
[f] Department of Geographical Sciences, University of Maryland, College Park, MD 20742, USA

ARTICLE INFO

ABSTRACT

Drainage networks composed of small, channelized ditches are very common in the eastern United States. These are human-made features commonly constructed for wetland drainage and constitute the headwater portion of permanent hydrographic networks. Accurate information on the drainage ditch location can help define where wetlands have been drained and evaluate impacts of artificial drainage patterns on hydrologic changes. Traditional water channel extraction approaches often cannot accurately identify small ditches especially in low-relief agricultural landscapes. In this study, we employed a state-of-the-art deep learning (DL) approach to extract drainage ditches using light detection and ranging (lidar) data in a low-relief agricultural landscape within the Delmarva area. First, we adopted a deep convolutional neural network based on U-Net architecture to classify ditches from different combinations of aerial optical and lidar derived (i.e., topographic and return intensity) features. The classification results were compared with a typical pixel-oriented machine learning classifier, random forest (RF). Next, we improved the connectivity of ditch networks through a minimum-cost approach and a further incorporation of FA to connect with natural drainage networks. Finally, we evaluated the connected drainage networks against flowlines derived from typical flow routing method (D8), an open-source channel network extraction tool (GeoNet), and the U.S. Geological Survey National Hydrography Dataset High Resolution data at 1:24,000 scale. Our results show that the DL model significantly outperformed the RF model, and the lidar derived topographic features were the most important input for ditch classification. The connected drainage networks extracted with DL exhibited pronouncedly higher precision (0.88) and recall (0.89) and a higher positional accuracy (within one pixel) than other flowline products. Overall, this study demonstrates the utility of DL approaches for automated extraction of ditch networks and the important contribution of lidar-derived topographic data for operational drainage network mapping at local and regional scales.

1. Introduction

Drainage networks composed of small, channelized ditches are usually represented by linear and regularly distributed features and are mostly human-made elements in low-relief agricultural landscapes (Bailly et al., 2008; Cazorzi et al., 2013; Dollinger et al., 2015). Extensive drainage ditch networks are quite common along the East Coast of the United States and are typically a result of extensive practices of grid ditching for mosquito control and drainage of wetlands for large-scale agriculture (Jones et al., 2018; McCarty et al., 2008). The drainage ditch networks can alter hydrologic connectivity at large scales and affect the status and function of wetlands by connecting wetlands and streams (Cohen et al., 2016; Lang et al., 2012b). It is reported that agricultural drainage through ditching and tiling has led to the greatest

---

* Corresponding authors.

loss of wetlands globally and the majority of wetland loss within the United States has occurred through drainage (Bartzen et al., 2010; Blann et al., 2009; Stedman and Dahl, 2008). These ditches are also linked to habitats for animals and plants, and the transport of nutrients and sediments from poorly drained depressional areas (drained wetlands) which can serve as critical source areas to downstream waters (Herzon and Helenius, 2008). The resultant increased nutrients and sediments flows can influence water quality and result in substantial biodiversity consequences in the lower catchment area (McCarty et al., 2008). Thus, headwater ditches represent hydrologically and ecologically important drainage elements that link their surrounding agricultural landscape to large, downstream waters. Accurate and efficient mapping of ditch networks is essential to determining drainage densities and magnitudes for quantifying where wetlands have been drained in agricultural landscape and improving understanding of watershed-scale hydrological interactions.

Hydrographical datasets, such as the U.S. Geological Survey (USGS) National Hydrography Dataset (NHD), are highly valuable at national and regional scales, providing a common reference of digital water drainage networks with features such as rivers and streams for the United States (Moore and Dewald, 2016). This dataset originated from USGS topographic quadrangle maps based on interpretations from stereo orthophotographs and field surveys and have been produced with a scale from 1:100,000 to 1:24,000 or more resolved, e.g., NHD Plus and NHD High Resolution. However, it has long been reported that commonly used stream network maps, like the NHD, underestimate actual stream length and provide limited information on extensive agricultural drainage ditches in headwater regions (Fritz et al., 2013; Hansen, 2001; Heine et al., 2008; Lang et al., 2012b; Persendt and Gomez, 2016). The headwater streams and ditches at the upstream extent of a watershed may be far more numerous than previously thought (Lang et al., 2012b; Nadeau and Rains, 2007). Since headwater streams and ditches are typically narrower, shallower, and in some cases heavily vegetated and temporarily inundated, it is challenging to use conventional mapping methods to detect their full length. This is especially true in areas of low topographic relief and areas where hydrography has been altered by humans due to development and other redirections of flow (Cazorzi et al., 2013; Elmore et al., 2013; Lang et al., 2012b).

In recent years, airborne light detection and ranging (lidar) data have emerged as a new and effective tool to capture subtle changes of local terrain and allow for automatic delineation of flow networks across large areas (Bai et al., 2015; Flyckt et al., 2022; Hooshyar et al., 2015; Lang et al., 2012b; Lindsay and Dhun, 2015; Wu et al., 2021). Airborne lidar produces three-dimensional point cloud products, including elevation data (XYZ), returned intensity values (relative strength of the return pulse), and in some cases RGB values from simultaneously acquired aerial images for each georeferenced point near the Earth's surface. It can be used to produce a map of bare earth high-resolution digital topographic products, such as digital elevation models (DEM) with buildings and vegetative canopy removed. These data have been widely used for extracting flow directions, topographic depressions, and channel networks (O'Neil et al., 2019; Wu et al., 2018). Moreover, lidar intensity can be effective in identifying inundation and channel networks owing to the strong absorption of incident near-infrared (NIR) energy by water relative to dry uplands (Hooshyar et al., 2015; Lang et al., 2020). The extraction of high-precision drainage networks utilizing lidar data has become a subject of keen interest for water resource managers and researchers aiming to develop and update hydrographical knowledge of landscapes (Poppenga et al., 2013).

To date, hydrologic modeling using flow routing methods based on gridded DEMs dominates in large-scale drainage network extraction given its simple form, efficient computational design, and hydrological continuity (O'Callaghan and Mark, 1984; Tarboton, 1997; Zhang et al., 2021). The general procedures of flow routing methods include filling pits, computing flow direction, and computing the contributing area draining to each grid cell, as well as defining a minimum contributing area threshold that forms a linear drainage feature (Stanislawski et al., 2017). Standard software tools such as Esri ArcGIS® Spatial Analyst Tools, and the System for Automated Geoscientific Analysis (SAGA) support the extraction of surface water drainage networks from DEMs using multiple flow routing methods such as D8 and D-infinity (Tarboton, 1997). Though flow routing methods have been widely used in drainage system analytics, such models have multiple limitations. The flow direction approach is less effective in low relief areas, where instead of allowing water to flow in any direction naturally, commonly used methods constrain water to only flow from one pixel to one or more adjacent pixels, increasing the likelihood of predicting false flow paths, especially for low relief landscapes and when using large-scale DEMs. In addition, the delineation of drainage networks from flow paths requires a unique threshold that is generally not able to fully reproduce the actual network (Li et al., 2020a; Passalacqua et al., 2010a). Orlandini et al. (2011) demonstrated how classic flow routing approaches are subject to variable reliability and sensitivity over different drainage basins and grid cell sizes with a general tendency to overestimate the network, and that they do not provide reliable predictions of channel heads across drainage basins with different types of morphology and channel initiation. Thus, subsequent manual edits are usually required to modify the flowlines generated from flow routing methods (Lang et al., 2012b).

Moreover, morphometric methods rather than hydrologic modeling are recommended to identify drainage networks in low relief landscapes (Gardner et al., 2007; Passalacqua et al., 2010a; Roelens et al., 2018a). Topographic metrics such as curvature, openness, and local relief, derived from DEMs often better define flow paths and are useful for the detection of local linear features at different spatial scales (Cazorzi et al., 2013; Pirotti and Tarolli, 2010; Roelens et al., 2018b; Sofia et al., 2011). Passalacqua et al., (2010a) developed a geometric framework (GeoNet) for automatic extraction of channel networks from high resolution data, in which likely channelized pixels are primarily identified by curvature and flow accumulation (FA) thresholds in combination with a geodesic minimization approach for channel network identification. However, automatic detection of drainage networks using morphologic features remains a challenge due to the multi-scale nature of geomorphological processes and the absence of objective thresholds for feature classification using a small set of features (Sofia et al., 2011). To overcome this hurdle, machine learning classifiers, such as random forest (RF), have also been applied to improve the detection of ditches by integrating multiple lidar derived optical or morphometric features (Flyckt et al., 2022; Roelens et al., 2018a). However, machine learning approaches based on morphometric features are primarily pixel oriented and don't consider the spatial context of features in input images, often leading to strong "salt-and-pepper" noise (Flyckt et al., 2022). Thus, a post-processing step of noise removal or ditch object construction is required to generate a clean drainage network. Object-oriented classifiers that utilize both pixel and contextual information (such as size, position, and shape) have also been applied to ditch mapping, leading to better ditch object recognition by aggregating pixels with similar properties into one category (Rapinel et al., 2015). However, the conventional object-oriented classification methods require two steps, image segmentation and classification, which disrupt the end-to-end workflow and are usually very complicated and involve various software packages.

With the emergence of graphic processing unit (GPU) configurations, rapid advances in deep learning (DL) have been widely acknowledged and adopted in computer vision tasks, such as challenging pattern recognition and object detection. Recently developed deep convolutional neural networks (DCNN) have demonstrated improvement in accuracy and efficiency for learning high-level contextual information from high resolution images. Several semantic network architectures, e. g., DeepLab, SegNET, and U-Net, have been developed and applied in classification tasks, such as urban and land use feature detection (Dang et al., 2020; Du et al., 2020; Pouliot et al., 2019). The DL approach has

been considered to have the potential to replace traditional object-oriented approaches in land cover classification and mapping (Zhang et al., 2020). Some pioneering efforts have explored DL techniques for extraction of geometric and hydrologic features, such as roads (Balado et al., 2019; Cira et al., 2020; Yang et al., 2019) and channels (Mao et al., 2021; Stanislawski et al., 2018; Xu et al., 2021), but limited effort has been undertaken, to our knowledge, to apply DL to extract small, channelized ditch networks from lidar data in low relief landscapes.

In this study, we employed a state-of-the-art DL model based on U-Net architecture to facilitate extraction of channelized ditches from lidar data in a low relief landscape within the Delmarva Peninsula in the eastern United States. A semi-automated stream reference product containing detailed headwater ditch information (either perennial or intermittent flow features) was used as the benchmark ditch reference. We investigated different combinations of aerial optical and lidar derived (i.e., topographic and return intensity) features for ditch classification and compared DL with a traditional pixel-oriented RF classifier. We further enhanced drainage network connectivity using a minimum-cost connection approach and FA to connect with natural drainage networks. Finally, we evaluated the connected drainage networks against flowlines derived from typical flow routing method (D8), an open-source channel network extraction tool (GeoNet) (described in section 2.5.2), and the USGS NHD High Resolution data at 1:24,000 scale. Our specific objectives include: 1) evaluate the potential of the DL method in ditch classification and compare its performance to a typical pixel-oriented classification method (i.e., RF); 2) investigate the role of different optical and lidar derived features in ditch classification; and 3) improve drainage network connectivity as compared with common existing flowline products.

2. Materials and methods

2.1. Study area

Our study area is located within the headwater region of the Upper Choptank River watershed on the Delmarva Peninsula in the eastern U.S. (Fig. 1). This region is characterized by thousands of vegetated depressional wetlands in a low relief agricultural landscape. The mean elevation of the Upper Choptank River watershed is ~16 m (maximum of ~46 m) above sea level, and the mean slope is less than 2° (Fig. 1). It has a humid, temperate climate with an average temperature of 2 °C in January-February and 25 °C in July-August. Rainfall is distributed nearly uniformly throughout the year (~1200 mm/yr) (Ator et al., 2005; Shedlock et al., 1999). The soils are largely derived from late Pleistocene fluvio-deltaic coastal plain and eolian sediments and are dominated by poorly drained soils in lower wet areas and better-drained (moderately well and well drained) soils in topographically higher uplands (Lowrance et al., 1997). Due to low relief and suitability of soils for ditch
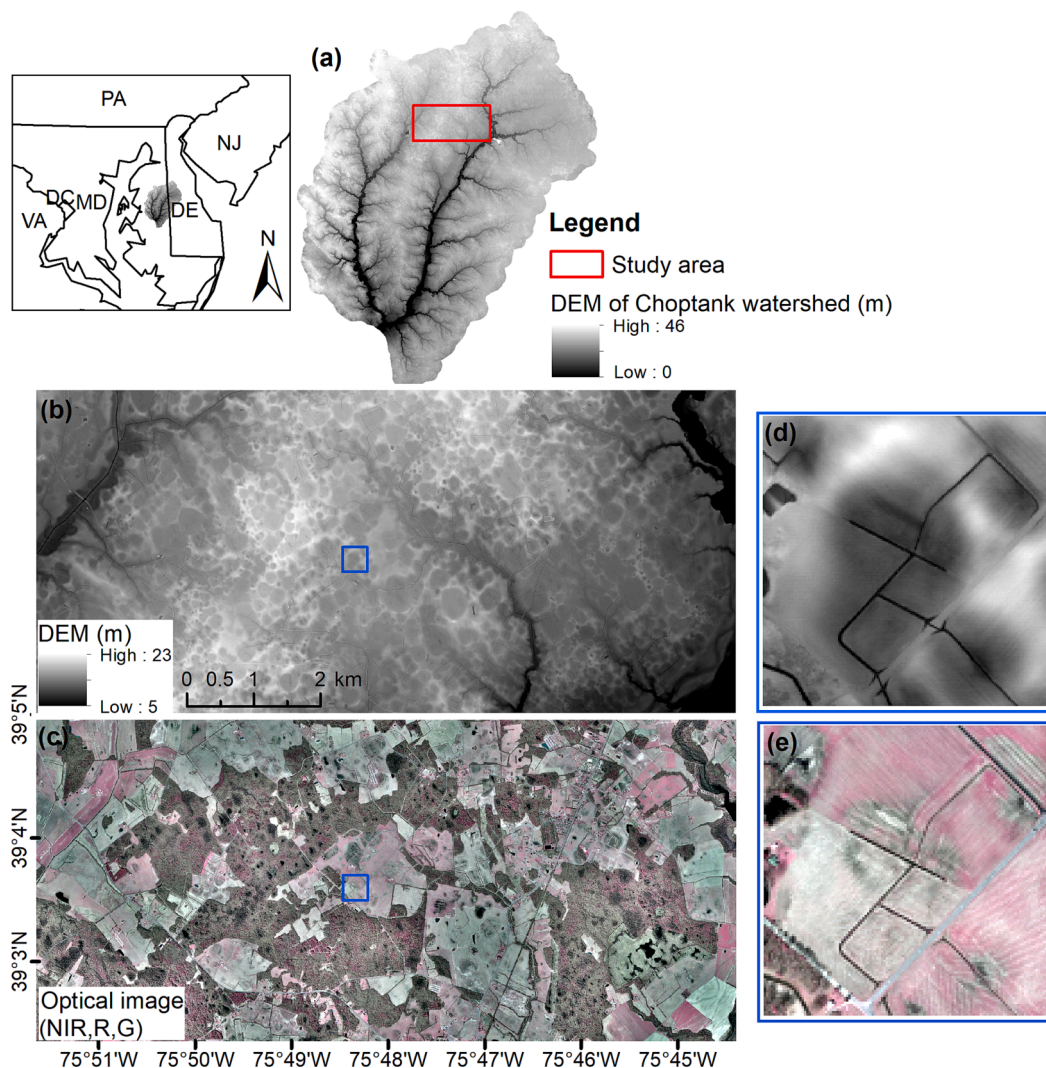
Fig. 1. Location of study area within the Upper Choptank River watershed (a). (b) and (c) are the DEM derived from lidar data, and optical image, respectively, for the study area. (d) and (e) illustrate small, channelized ditches that are commonly present in depressional areas.

drainage, the majority (58 %) of depressional wetlands have been converted or drained with extensive ditches to allow for agricultural cultivation (i.e., prior converted croplands), primarily corn and soybean production (Benitez and Fisher, 2004; McCarty et al., 2008). In total, cropland (as the dominant land use type) covers about 60 % of the Choptank River watershed, with a smaller amount of forest (26 %) and urban area (6 %) (Fisher et al., 2006).The drainage ditches are often seasonally inundated, and the putative role of a channel for water movement is indicated by its connectivity to larger flow channel networks.

2.2. Airborne lidar data and derived features

We obtained the lidar flight campaign data of 2007 for the study area (Fig. 1). Three types of lidar features were derived for ditch classification, including topographic (T), intensity (I), and optical (O) features (Figs. 2-3), which are detailed in the following sections.

2.2.1. Topographic features

We used the DEM that was derived from the lidar data collected on December 24, 2007, when minimal inundation was present in the headwater region (Fig. 1). The Leica ALS50-II sensor with 1064 nm wavelength was flown at 1,829 m above the Earth's surface to collect elevation and intensity data. Data were collected with a pulse rate of 126,000 Hz and scan frequency of 50 Hz per second with a scan angle of $+/-25°$. The product has a vertical accuracy of ≤ 0.15 m and a pulse density of ~2.8 pts/m^2 (~0.35 m post spacing). Bare earth point elevations of bridges and other obstructions that can lead to inaccurate water routing were manually identified and lowered to the level of flowing water using LP360 software. Inverse distance weighted (IDW) interpolation was used to produce a 3 m gridded DEM. A more detailed description of this data collection and processing is available in Lang

et al., (2012a).

Topographic metrics including general curvature (GC), topographic positive openness (TPO), and topographic wetness index (TWI) were derived from the December lidar DEM using SAGA v. 7.3.0. As mentioned previously, the GC and TPO have been widely utilized to extract channel networks. They represent primary metrics directly calculated from elevation and describe local surface geometry or relative position of a given point (Li et al., 2020b). TWI is defined as a function of local upslope contributing area and slope, which represents a secondary (combined) metric (Li et al., 2020b), and has been commonly used in other studies to quantify local topographic control on hydrological processes (Du et al., 2021; Lang et al., 2012a).

2.2.2. Intensity features

We used lidar intensity data obtained over the same study site on March 27, 2007, a period of average maximum hydrologic expression in early spring, to test the utility of lidar intensity for ditch classification. The Optech Airborne Laser Terrain Mapper (ALTM) 3100 lidar sensor was flown at 610 m above the Earth's surface to collect elevation and intensity data for the study area. Data were collected with a pulse rate of 100,000 Hz and scan frequency of 50 Hz per second with a scan angle of $+/-20°$. For each laser pulse, up to 4 returns were recorded (i.e., first, second, third, and ground) and intensity of each return was captured with a 12-bit dynamic range. The lidar data had an overall vertical accuracy of ≤ 0.15 m and an average point density of ~2.5 pts/m^2 (0.40 m post spacing). A digital camera was used to capture coincident aerial photography including the NIR (720–920 nm), red (600–720 nm), and green (510–600 nm) bands. A more detailed description of this March lidar data collection and processing is available in Lang and McCarty (2009) and Lang et al., (2012a).

We used the first and ground return lidar intensity raster images which were interpolated and filtered by Lang et al. (2020). To exclude
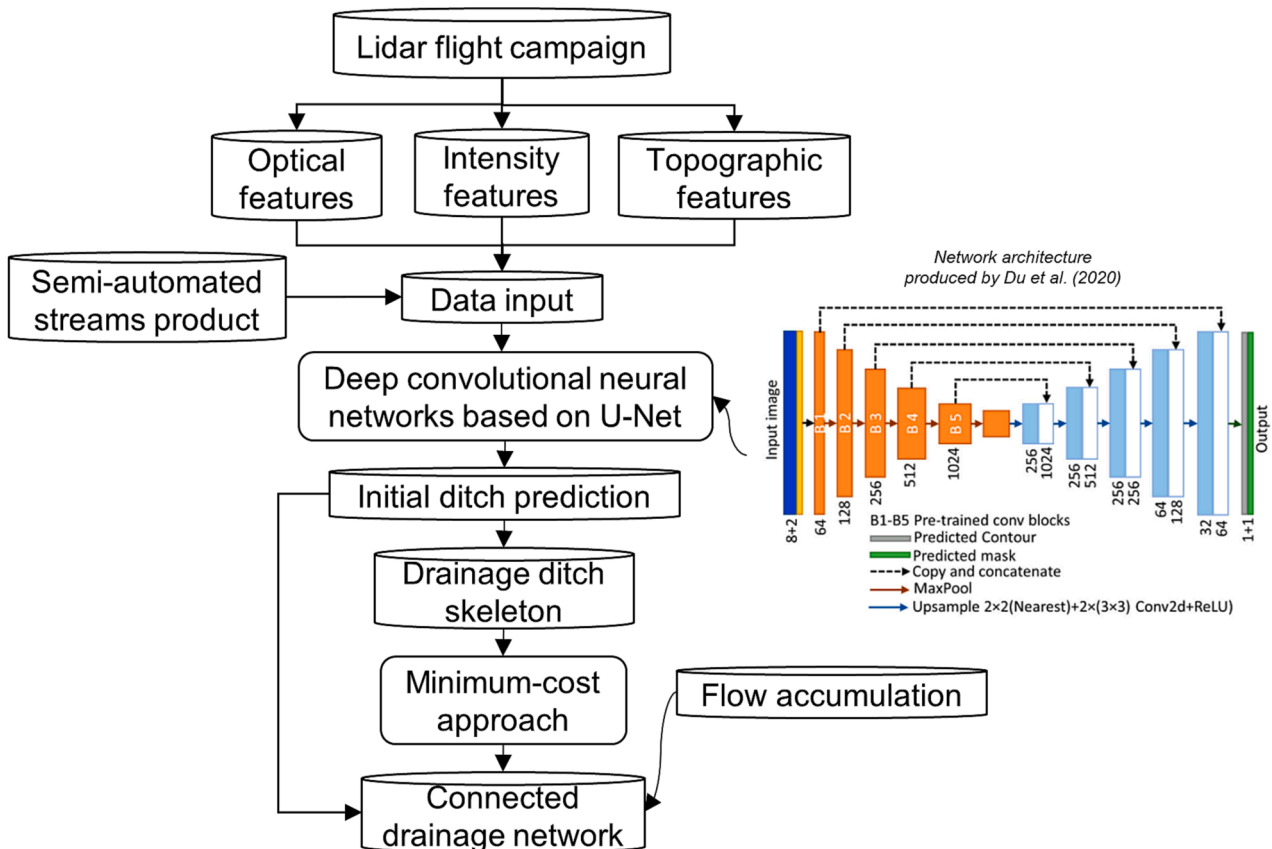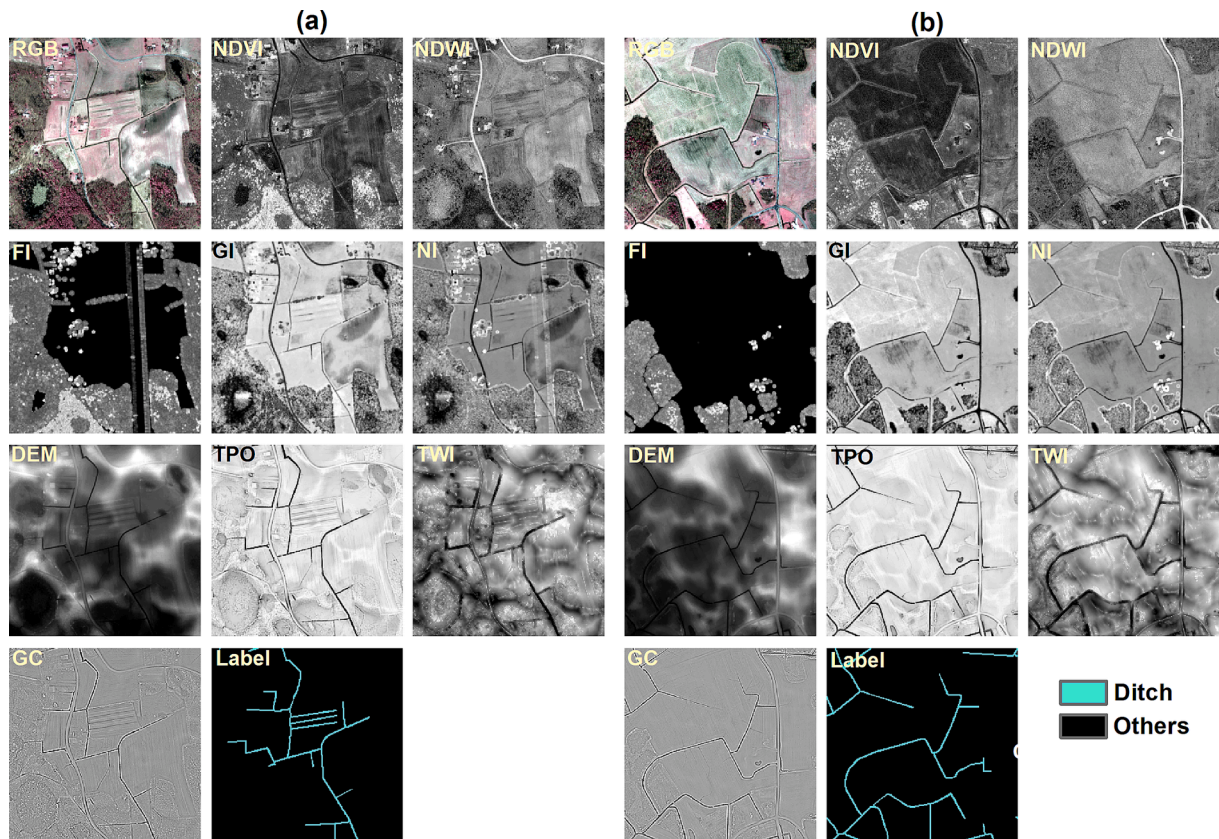

Fig. 2. Workflow of drainage ditch network extraction from lidar data.

Fig. 3. Image patches of optical and lidar derived (i.e., topographic and return intensity) features with ditch reference labels for two example areas (a and b). RGB: NIR, red, green bands; NDVI: Normalized Difference Vegetation Index; NDWI: Normalized Difference Water Index; FI: first return intensity; GI: ground return intensity; NI: Normalized Intensity; DEM: Digital Elevation Model; TPO: Topographic Positive Openness; TWI: Topographic Wetness Index; GC: General Curvature. (For interpretation of the references to color in this figure legend, the reader is referred to the web version of this article.)

the effect of evergreen vegetation on inundated surface, which can be confused with inundation within ground lidar intensity images, we also employed the normalized intensity using the technique described in Lang et al. (2020). The normalized intensity has been shown effective in delineating forested wetland inundation (Du et al., 2020).

2.2.3. Optical features

The utility of optical data for ditch classification was investigated using the March aerial photography data which included the NIR, red, and green bands. Based on these bands, the Normalized Difference Vegetation Index (NDVI) and Normalized Difference Water Index (NDWI) were calculated (Equation (1) and (2). These two indices have been widely used for differentiating water surface features from soil and vegetation.

$$NDVI = \frac{NIR - Red}{NIR + Red} \tag{1}$$

$$NDWI = \frac{Green - NIR}{Green + NIR} \tag{2}$$

2.3. Semi-automated stream reference

We used the semi-automated stream product derived from lidar data by Lang et al., (2012b) as the benchmark, which includes perennial and intermittent streams and ditches at the headwater region of the Choptank watershed and was shown to be more inclusive of the lower order stream/ditch network than the NHD product. This semi-automated stream product was generated by automatic extraction of stream networks based on FA followed by detailed manual editing. In this study, a 3-m buffer was generated along the semi-automated streamlines to

estimate the width of ditch channels.

2.4. Initial ditch classification

2.4.1. Deep learning network architecture and ditch classification

We employed the novel DCNN established by Du et al. (2020) based on U-Net architecture to classify ditches using different input combinations, i.e., O, I, T, O + I, O + T, I + T, O + I + T (Figs. 2-3). U-Net is a sophisticated symmetric "U" type fully connected CNN, which was initially proposed by Ronneberger et al. (2015) to solve the biomedical imaging partition problem. U-Net structure consists of the encoder blocks, accounting for extracting deep hidden features from the input image by passing several convolution-pooling operations, and the decoder blocks that aim to produce pixel-level segmentation by recovering hidden features to the original image size through up sampling. Due to the special "U" type, U-Net often achieves high accuracy when solving image segmentation problems and has been the most widely used semantic segmentation structure in recent years. In this study, our U-Net based DL model combines the most recent components that maximize the performance of per-pixel classification, including 1) a U-Net backbone architecture, 2) use of modified residual blocks of convolutional layers in architecture, and 3) a hybrid loss function combining the Dice loss and Focal loss to facilitate model training. Segmenting small-size objects is always challenging due to imbalanced data distribution. In our case, the small ditches are much smaller than non-ditches, leading to model training challenges. The combined loss function outperforms simple Dice or focal loss functions in addressing extremely imbalanced data and gauging the similarity between samples of prediction and ground truth (Zhu et al., 2019). Our ditch classification with the DL model included three steps: model training, image

classification, and classification assessment. The ditch buffers generated from the semi-automated streams product were used to generate ditch labels for model training.

For model training, ditch labels were binarized with the ditch pixels represented as "1″ and the non-ditch pixels as "0". The ditch labels combined with optical and lidar derived features were further split into small image patches to allow for model training because DL model training is computationally intensive with entire remote sensing images. We used a simple sliding window (256*256) to split entire images and the overlap rate of the sliding window was set to 0.5 to increase the number of image samples. To further expand our training data, four types of data augmentation (rotate 90○, rotate 180○, rotate 270○, and flip) were applied to each split image patch. Finally, we generated 315 image patches that contain ditches, and randomly selected 63 (20 %) for model training and the remaining 252 (80 %) for validation. Our DL model was trained using the PyTorch framework. Model training was carried out on a computer with Intel(R) Xeon(R) Gold 6136 CPU @ 3.00 GHz (48 CPUs) and NVIDIA Quadro P6000 GPU. Python libraries including fastai, scikit-image, GDAL, and NumPy, were used in our workflow.

2.4.2. Classification assessment

We compared the initial DL classification results with pixel-oriented classification based on RF classifier. The RF method is often considered to outperform other machine learning methods and have been widely applied to classification tasks. In our study, the RF classification was performed using the "randomForest" package in R (Liaw and Wiener, 2002). We used constant ntree (the number of trees) of 500, and mtry (the number of variables at each split) equaled the square root of the number of total inputs. We used the same training and validation dataset that was used for DL classification to train and assess the RF model. The classification performance of DL and RF based on different input combinations was evaluated at both the pixel level using the confusion matrix and the object level using the intersection over union (IoU) metric.

We calculated Precision, Recall, and F1 score using the validation dataset for pixel level assessment. Precision represents the portion of pixels that are correctly classified as ditches (Equation (3), while Recall denotes the model's ability to capture all ditch pixels from the reference data (Equation (4). A reliable classification is expected to have both high Precision and Recall, which in return results in a high F1 Score (Equation (5).

$$Precision = \frac{TP}{TP + FP} \times 100 \qquad (3)$$

$$Recall = \frac{TP}{TP + FN} * 100 \qquad (4)$$

where *TP* is the number of true positives (i.e., ditches in reference labels correctly identified as ditches). *FP* is the number of false positives (i.e., non-ditches in reference labels identified as ditches), and *FN* is the number of false negatives (i.e., ditches in reference labels not identified).

$$F1_{score} = 2 \times \frac{Precision \times Recall}{Precision + Recall} \qquad (5)$$

To assess the accuracy of ditch classification at object level, we adopted a metric based on the intersection over union (IoU), also known as the Jaccard index. This is the ratio of overlapped area to the area of union between prediction and reference for a category (Equation (6) (Choi et al., 2010). The value of IoU ranges from 0 to 1, and an IoU of 0.5 or above is usually considered satisfactory results.

$$IoU(A, B) = \frac{Area(A \cap B)}{Area(A \cup B)} \qquad (6)$$

where *A* and *B* correspond to ditches predicted from DL and in reference

labels, respectively, in this study.

2.5. Drainage connectivity improvement

2.5.1. Ditch connection algorithms

The previous step resulted in an initial prediction of ditches from the DL model, which was a ditch probability map represented by softmax values for each pixel. Ditch skeletons were created by thresholding the ditch probability and then using the skeletonize function in Python to generate ditch centerlines. The initial connection of ditch segments in our study is equivalent to finding a minimum cumulative cost path connecting two points based on the ditch probability map and ditch skeletons. We first excluded ditch skeletons with length ≤ 5 pixels to reduce computation complexity. For each ditch skeleton, we identified the starting point (the most downstream point with a low elevation value) and the ending point (the most upstream point with a high elevation value). From the endpoint of each ditch skeleton, we detected the closest vertices that have higher elevation values within a search radius of 100 m, and the minimum-cost path was selected as the potential connection segment. Note that the averaged connection probability should be greater than a selected threshold and the potential connecting segment cannot cross other ditch segments.

To further improve the connectivity at the intersection of ditch networks or the occlusion parts caused by bridges and other obstructions that are not connected by minimum-cost approach, we incorporated FA information to connect ditch segments with the major natural drainage network. Based on the initially connected ditches, we again identified the starting point (the most downstream point with the highest FA value) of each ditch network. From each starting point, we detected and traced the adjacent pixel with the highest FA value until a ditch pixel was encountered in a search radius of 500 m. In our study, FA was generated from the D8 algorithm using "whitebox" R package.

2.5.2. Evaluation of connected drainage ditch network

We evaluated the performance of the connected drainage network by comparisons with flowlines derived from typical D8 flow routing method and GeoNet tool as well as the existing NHD High Resolution product at 1:24,000 scale. By checking the histogram of the FA for randomly selected ditches (approximately 50 ditch sources) in depressional areas, we found that most ditch source pixels had a FA range of 1 ~ 4 ha. Thus, we selected 1 ha as the minimum FA threshold to automatically extract ditch flowlines based on D8 method. The GeoNet tool has also been demonstrated an effective tool to map channel heads and networks in either mountainous or flat landscapes (Passalacqua et al., 2012; Passalacqua et al., 2010b). We tested the latest MATLAB version of GeoNet (GeoNet_v2.2) downloaded from GeoNet google site (available at https://sites.google.com/site/geonethome/) for automatic extraction of channel flowlines. Because our study area is flat, we switched to Laplacian curvature in GeoNet which is recommended by Passalacqua et al. (2012) for channel network extraction in flat landscapes, and the adjustable flowThresholdForSkeleton parameter was also set to 1 ha to remove convergent areas with contributing area below this threshold.

For comparison, we also calculated the Precision and Recall for each flowline product according to Equation (3) and (4). Note that, here, TP is defined when the 7*7-pixel window of a predicted ditch pixel is traversed by the reference ditch centerline. FP represents the case when the 7*7-pixel window of a predicted ditch pixel is not traversed by the reference ditch centerline. FN occurs when the 7*7-pixel window traversed by the actual ditch centerline cannot find a ditch prediction, i.e., a reference ditch pixel is not identified. In addition to Precision and Recall, we also calculated the distance error (D_k) for each ditch product, which is the Euclidean distance between the predicted ditch pixel (C) and the closet pixel (P) in the reference (Chen et al., 2020; Moretti and Orlandini, 2018). The distance error is defined as:

$$D_k = \sqrt{\left(x_k^{(c)} - x_k^{(p)}\right)^2 + \left(y_k^{(c)} - y_k^{(p)}\right)^2} \tag{7}$$

where $k = 1, ..., N$ which represents each predicted dich pixel. N is the total number of ditch pixels identified. Then, the mean Euclidean distance error $E(D)$ can be calculated as

$$E(D) = \frac{1}{N} \times \sum_{k=1}^{N} D_k \tag{8}$$

3. Results

3.1. Comparison of deep learning and random forest for ditch classification

At the pixel level, there was a significantly higher classification accuracy using the DL than that using RF. The F1 score of all different optical and lidar feature combinations for DL was higher than that using RF (Table 1). The highest F1 score (0.69 ~ 0.71) occurred for the DL model when lidar topographic features are included (i.e., T, O + T, I + T, O + I + T). In contrast, without topographic features (i.e., O, I, and O + I), DL achieved F1 score of 0.45 ~ 0.53. For RF, higher F1 scores (0.37 ~ 0.41) also occurred with topographic features, and F1 score dropped to 0.09 ~ 0.14 without topographic features. For each data input, the Precision of DL was significantly higher than that of RF, while the Recall of DL was lower than that of RF (Table 1).

At the object level, by visual inspection, the ditch objects predicted from DL generally showed a clearer pattern of linear features and less speckles than those from RF (Figs. 4-5). This finding is supported by the higher IoU values of DL results. The ditches classified by DL matched the ditch labels very well and achieved the highest IoU values (0.53–0.56) with the inclusion of topographic features (Table 1 and Fig. 4). The highest IoU for RF was only 0.23–0.26 with topographic features included, and there were strong "salt-and-pepper effects" in predictions, especially for data inputs without topographic features (Table 1 and Fig. 5).

3.2. Enhanced drainage network connectivity

The drainage connectivity of ditches from initial DL prediction was improved by two steps: a minimum-cost connection approach and a further incorporation of FA (Fig. 2 and Fig. 6). Potential ditch segments between ditch vertices and in the intersection portions of ditch networks were successfully detected while small ditch noise was excluded (Fig. 6d, h).

In comparison with the flowlines derived from typical D8 method, the GeoNet tool, and the NHD High Resolution product at 1:24,000 scale, our connected drainage network showed the highest Precision (0.88) and Recall (0.89) (Table 2) and well reproduced ditch patterns in reference labels (Fig. 7). The total length of our connected drainage networks in the study area was 163 km, which was also comparable to the length of the labeled ditches (160 km). For GeoNet, it showed moderate Precision (0.62) and Recall (0.60) with a ditch length of 157

km (Table 2). There were obvious errors of omission (false negative) and commission (false positive) in channel extraction using GeoNet (Fig. 7). The drainage flowline derived from the D8 method was more likely to be committed than omitted (Recall was 0.82, Recall was only 0.43) and almost doubled in the total length with lots of meandered centerlines generated around the actual ditches. Given the large 1:24,000 scale, NHD data were sparse and only included major channels in the study area. Not surprisingly, the NHD data exhibited a substantial underestimation in drainage length (79 km), contributed by the lowest Precision (0.32) and a moderate Recall (0.65) (Table 2 and Fig. 6). Moreover, the mean distance error of our connected drainage network was the lowest (2.17 m, less than the side length of one pixel) followed by the typical D8 method, with the largest distance error for NHD flowlines (29.31 m).

4. Discussions

Extraction of drainage ditch networks in agricultural landscapes is important and challenging due to low local relief and complex hydrologic processes in headwater regions. The overall quality and utility of any drainage map is determined by its ability to represent these small headwater streams and ditches. As high resolution lidar data have become widely available from a variety of vendors during recent years, new opportunities for automatically extracting drainage network from lidar data at large scales are emerging. However, there are various limitations in automatic and accurate extraction of natural and artificial channel networks using traditional hydrologic or morphometric methods. In this study, we employed a state-of-the-art DL model based on U-Net architecture to classify ditches using different combinations of aerial optical and lidar derived features as inputs and further enhanced the drainage connectivity within the Upper Choptank River watershed. We found that the DL model has great potential for accurate ditch extraction compared to typical machine learning classification methods (i.e., RF) and demonstrated the importance of topographic features in ditch classification. The connected drainage network also outperformed the flowlines derived from typical flow routing method, the GeoNet tool, and the NHD High Resolution product. The effectiveness of DL models based on DCNN to fully utilize the contextual information from lidar data (especially topographic features) to detect small ditches is the primary strength of this study.

The DL model based on U-Net performed better in extracting ditch features with a clear pattern, whereas traditional classification methods such as RF failed to do so and resulted in considerable prediction noise (Figs. 4-5). There are mixed sources of noise associated with surface water or urban features such as roads in RF results (Fig. 5). Satisfactory prediction results using DL were demonstrated by both higher F1 scores and IoU values relative to RF (Table 1). High-resolution lidar data provide much more information about object-oriented contextual features than pixel-oriented spectral features. The DL model is object-oriented, allowing it to take both the pixel and multi-scale contextual information into consideration while extracting ditch information from lidar data. In contrast, RF classification is performed at the pixel level which often leads to strong "salt-and-pepper" noise and a mix of other

Table 1

Accuracy assessment of initial ditch classification using DL and RF. Bold fonts represent the highest F1 scores and IoU achieved from DL, with inclusion of topographic features. O: optical features; I: intensity features; T: topographic features; DL: deep learning, RF: random forest; IoU: intersection over union.

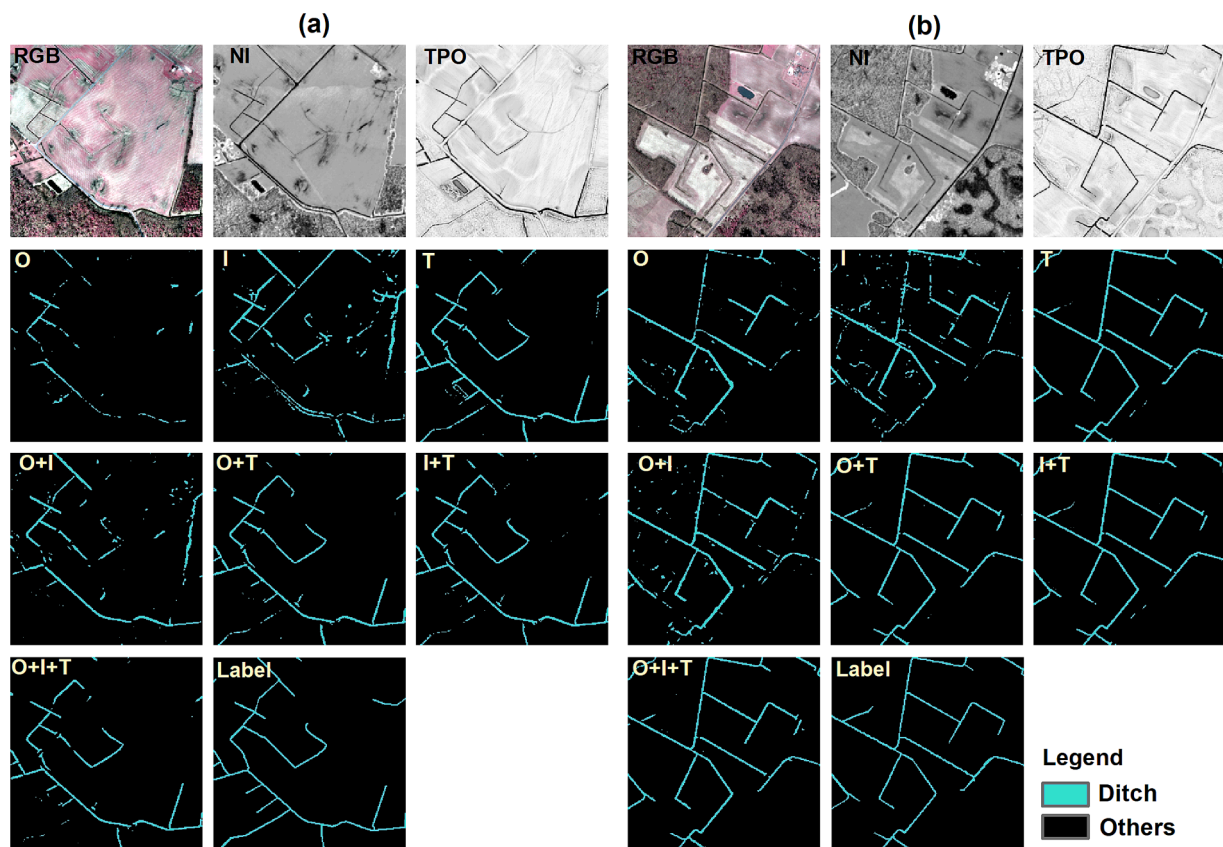| Data Input #	Lidar features			DL				RF			
	O	I	T	Precision	Recall	F1 score	IoU	Precision	Recall	F1 score	IoU
1	×			0.56	0.38	0.45	0.29	0.05	0.72	0.09	0.05
2		×		0.42	0.49	0.45	0.29	0.05	0.71	0.10	0.05
3			×	0.63	0.76	**0.69**	**0.53**	0.23	0.93	0.37	0.23
4	×	×		0.53	0.53	0.53	0.36	0.08	0.82	0.14	0.08
5	×		×	0.69	0.74	**0.71**	**0.55**	0.25	0.94	0.39	0.24
6		×	×	0.67	0.76	**0.71**	**0.56**	0.25	0.94	0.40	0.25
7	×	×	×	0.68	0.73	**0.70**	**0.54**	0.26	0.94	0.41	0.26

Fig. 4. Ditch classification results for two example areas using the deep learning model based on different input combinations (O: optical features; I: intensity features; T: topographic features). False color near-infrared imagery (RGB), Normalized Intensity (NI), and Topographic Positive Openness (TPO) are shown at the top for reference.

categories in ditch class. Thus, a second step of noise removal or ditch object construction is usually required through filtering or aggregation methods (Roelens et al., 2018a). In our study, though the RF model generated the highest Recall, its Precision was much lower than that of DL (Table 1), which indicates that RF can completely capture the ditches from the reference map but heavily overestimate the ditch class, leading to both low overall F1 scores and IoU estimates. Hence, we recommend the combined usage of IoU and overall accuracy for evaluation of classification models.

We obtained better classification results when the lidar derived topographic features (T) were included in both DL and RF models (Table 1, Figs. 4-5), showing the important contribution of topographic information in ditch classification for both models. We also found a generally greater relative importance of topographic features (i.e., TPO and DEM) than intensity and optical features using the RF model (Fig. 8). This suggests that the DL model holds promise to map perennial and intermittent ditch/stream networks at large scales solely based on topographic metrics without involvement of water-related indices. Though drainage ditch networks could be captured well using lidar topographic features and the DL model, the agricultural landscape introduced many challenges in capturing roadside ditches which were much narrower channels designed to convey stormwater away from transportation throughways. Potential roadside ditches can be more precisely inferred from higher resolution lidar DEM data.

The initial extraction of ditches with DL often generated good connectivity for main ditch networks with inclusion of topographic data (Fig. 4), which is consistent with the work of Xu et al. (2021) showing that the U-Net model achieves significantly better smoothness and connectivity between classified streamline channels relative to other machine learning methods. To enhance drainage connectivity between small ditches, we implemented a minimum-cost approach directly based

on initial ditch probability from DL to identify the potential connection between ditch segments. This was simpler than other reported connection models such as building a logistic regression model to add possible missing channel connections (Roelens et al., 2018a). The incorporation of FA information into the ditch segments could further improve hydrologic connectivity with the major natural drainage network where the accuracy of FA is relatively high. Our connected drainage network outperformed all other flowlines derived from D8 flow routing method, the GeoNet tool, and the NHD High Resolution product, in terms of Precision, Recall, total length, and distance error (Table 2). As expected, flow routing methods can generate good connectivity of flow paths and detect the natural network well, but they showed a broader ditch extent with many occurrences of channels (e.g., unchanneled preferential surface flows) in locations where ditch channels are not observed, resulting in a low Precision (0.43), and also failed to capture some truth dich channels (Fig. 7). This is in line with Orlandini et al. (2011), who found that there is a general tendency to overestimate the network using flow routine methods, and that they do not provide reliable prediction of channel heads across drainage basins. Though Passalacqua et al. (2012) documented that the GeoNet had the ability to distinguish channel heads in flat landscapes (i.e., Le Sueur River Basin, Minnesota) based on the Laplacian curvature, it still generated moderate errors of omission and commission in ditch extraction (Fig. 7). In GeoNet, the likely channelized pixels are primarily distinguished by thresholding the curvature first and then filtered by a FA threshold parameter to remove small convergent areas (unwanted noise). The classification errors of GeoNet can be likely caused by the reliance on FA to distinguish truth drainage pixels and noisy areas, because flow routine methods (D8 or D-Infinity) have large uncertainties in quantifying the drainage area in a super low relief landscape in our study area. Also, this tool requires filtering techniques (e.g., median filtering) to remove unwanted sources
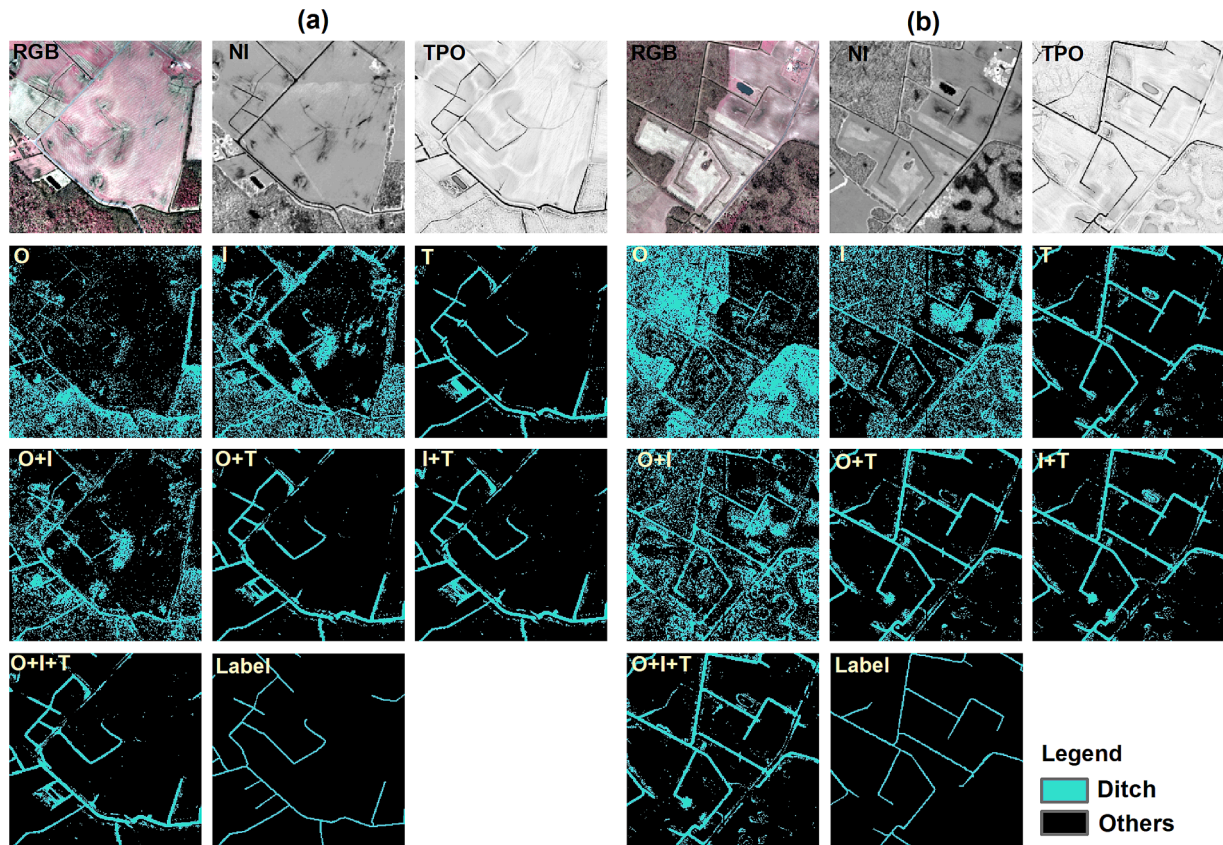
Fig. 5. Ditch classification results for two example areas using the random forest model based on different input combinations (O: optical features; I: intensity features; T: topographic features). False color near-infrared imagery (RGB), Normalized Intensity (NI), and Topographic Positive Openness (TPO) are shown at the top for reference.
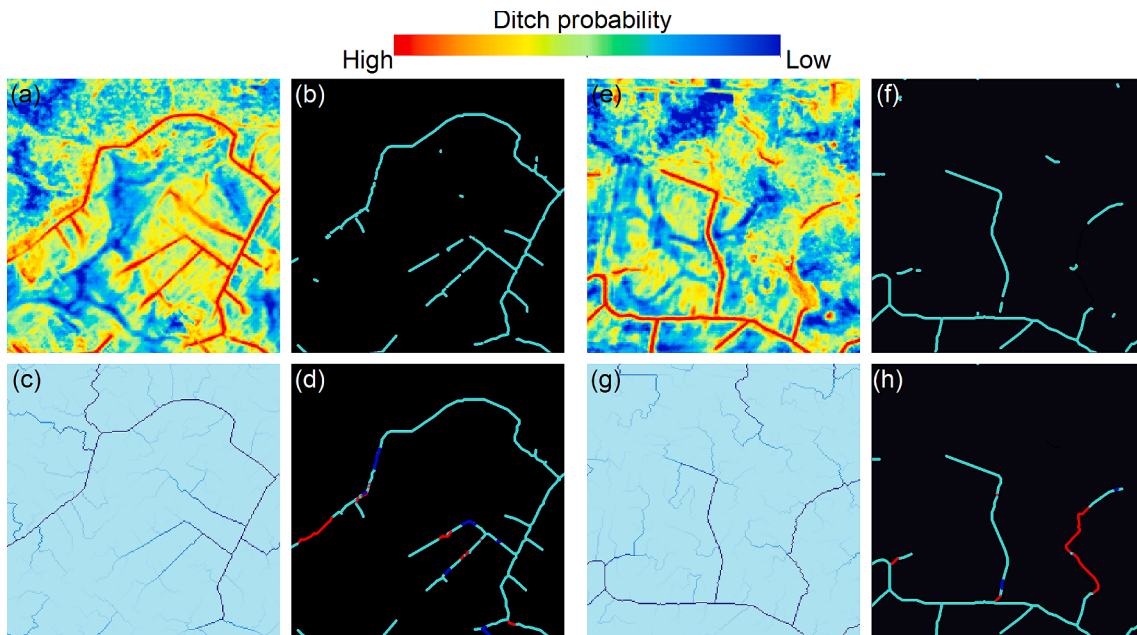

Fig. 6. Examples of enhanced drainage connectivity using the proposed connection methods. (a) and (e): the probability map of ditches represented by softmax values; (b) and (f): ditch skeletons obtained by thresholding predicted ditch probability; (c) and (g): flow accumulation based on the D8 algorithm; (d) and (h) connected drainage network. Blue segments were detected by minimum-cost connection approach, while red segments were incorporated from flow accumulation. (For interpretation of the references to color in this figure legend, the reader is referred to the web version of this article.)

Table 2
Summary statistics of the connected drainage network developed in this study using a Deep Learning (DL) model against other flowlines derived from typical D8, GeoNet v2.2 tool, and the NHD High Resolution at 1:24,000 scale.

Category	Precision	Recall	Distance error (m)	Length (km)
Label				160
DL (this study)	0.88	0.89	2.17	163
D8	0.43	0.82	4.82	312
GeoNet v2.2	0.62	0.60	6.17	157
NHD HR	0.65	0.32	29.31	79

of noise in raw elevation data processing (Sangireddy et al., 2016), with uncertainty in setting filtering window sizes. This highlights the advantage of the DL method based on DCNN in identifying detailed contextual information from high-resolution images while automatically excluding noisy features in results without filtering operations. In our study, a larger FA threshold (e.g., 2 ~ 5 ha) can result in more realistic ditch networks for both D8 and GeoNet methods, however, substantially omitted many ditches and shorten the extracted drainage network (results not shown). The NHD flowlines also provides a realistic and well-connected drainage network product, however, the large scale (1:24,000) of NHD only allows it to include major stream channels, and ignores smaller tributaries, leading to lower accuracy than the other products. Overall, the DL approach is superior to both pixel-oriented machine learning methods and existing automatic methods for extracting ditch features.

Despite the advantages of using DL in pattern recognition and object detection from images, preparing good quality training labels for DL models has proven challenging due to the scarcity of high-resolution reference data. In contrast, traditional pixel-oriented machine learning approaches (e.g., RF) only require a small number of point format training data. Note that results using RF were usually less satisfactory with lots of speckle noise. In our study, we employed the semi-automated stream product generated by Lang et al., (2012b) to represent the perennial and intermittent stream and ditch reference data for model training and validation. This was generated by combing the FA-derived stream network and extensive human edits (nearly half of the streams and ditches). This workflow is extremely time consuming and

requires extensive prior knowledge. In the future, it may be possible to use Self-Supervised Learning (SSL) technology to solve some of challenges posed by the over-dependence of semantic segmentation on labeled data (Hu et al., 2021). Moreover, there have also been some efforts in identifying ditches directly from 3D lidar point clouds that contain volume, accurate 3D information about the ground targets (Roelens et al., 2018a). The potential of DL models for improving ditch identification from 3D space could also be evaluated in future research.

5. Conclusions

Mapping channelized ditch drainage networks in headwater regions is essential but challenging using high resolution lidar data. In this study, we demonstrated the advantage of using a state-of-the-art DL model based on U-Net architecture to classify ditches in a low-relief landscape from lidar data. The use of minimum-cost connection approach and flow accumulation can further improve the connectivity of the DL generated ditch networks. The DL model significantly outperformed the traditional pixel-oriented RF model with significantly less "salt-and-pepper" effects. And lidar derived topographic features are essential for accurate ditch classification. The connected drainage networks also show higher accuracy (Precision = 0.88, and Recall = 0.89) and lower distance error (within one pixel) than flowlines derived from typical D8 method, the GeoNet tool, and the NHD High Resolution product. Our study demonstrated the benefits of using DL models to extract ditches from high resolution lidar derivatives and showed the potential of DL techniques to support future operational drainage network mapping at large scale.
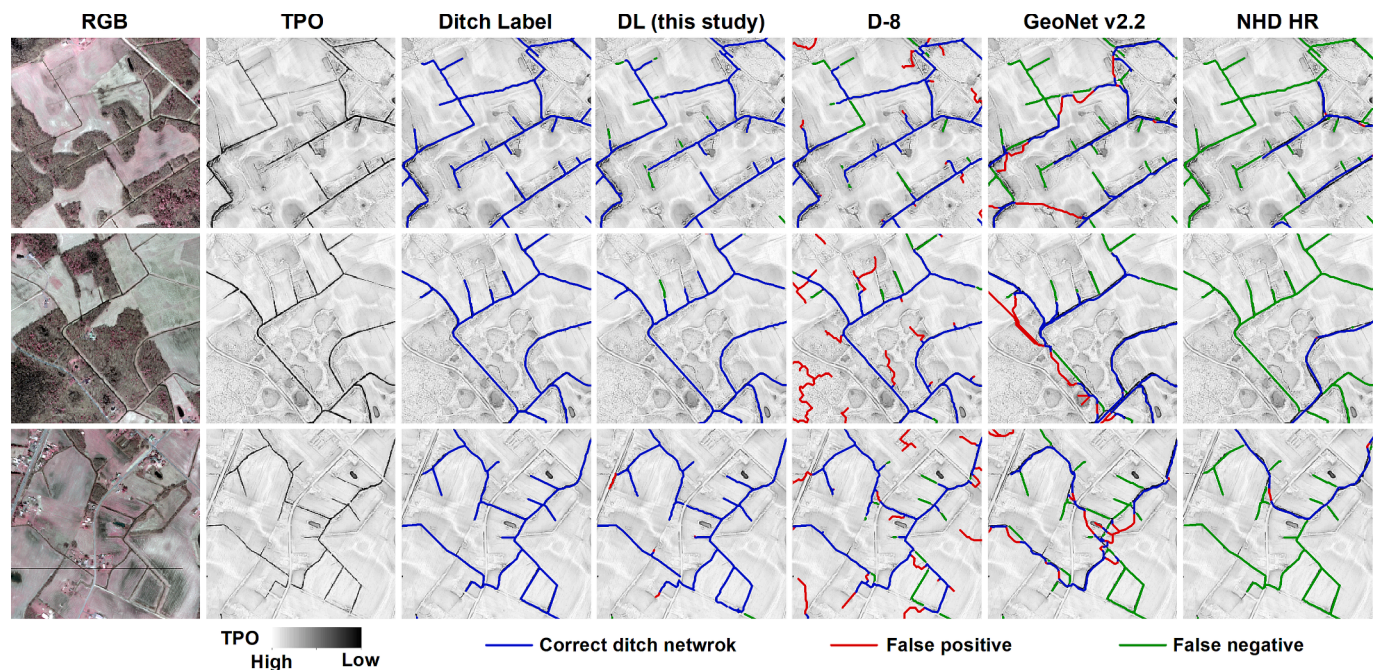
Fig. 7. Comparison of connected drainage network using deep learning (DL) in this study and flowlines derived from typical D8, GeoNet v2.2 tool, and the NHD High Resolution at 1:24,000 scale. RGB: false color near-infrared imagery, TPO: Topographic Positive Openness.
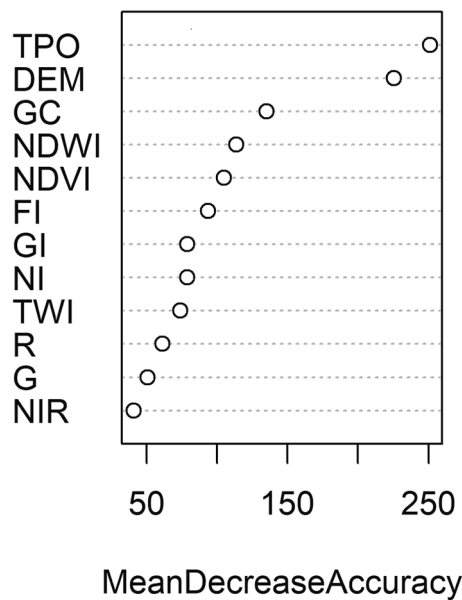
Fig. 8. Relative importance of different input features in the RF model for ditch classification. DEM: Digital Elevation Model, TPO: Topographic Positive Openness, GC: General Curvature, TWI: Topographic Wetness Index; NDVI: Normalized Difference Vegetation Index; NDWI: Normalized Difference Water Index; FI: first return intensity; GI: ground return intensity; NI: Normalized Intensity.

review & editing.

Data availability

Data will be made available on request.

References

Ator, S.W., Denver, J.M., Krantz, D.E., Newell, W.L., & Martucci, S.K. (2005). A surficial hydrogeologic framework for the Mid-Atlantic Coastal Plain. In, *Professional Paper*. Reston, VA.

Bai, R., Li, T.J., Huang, Y.F., Li, J.Y., Wang, G.Q., 2015. An efficient and comprehensive method for drainage network extraction from DEM with billions of pixels using a size-balanced binary search tree. Geomorphology 238, 56–67.

Bailly, J.S., Lagacherie, P., Millier, C., Puech, C., Kosuth, P., 2008. Agrarian landscapes linear features detection from LiDAR: application to artificial drainage networks. Int. J. Remote Sens. 29, 3489–3508.

Balado, J., Martinez-Sanchez, J., Arias, P., & Novo, A. (2019). Road Environment Semantic Segmentation with Deep Learning from MLS Point Cloud Data. *Sensors (Basel), 19*.

Bartzen, B.A., Dufour, K.W., Clark, R.G., Caswell, F.D., 2010. Trends in agricultural impact and recovery of wetlands in prairie Canada. Ecol Appl 20, 525–538.

Benitez, J.A., Fisher, T.R., 2004. Historical land-cover conversion (1665–1820) in the Choptank watershed, eastern United States. Ecosystems 7, 219–232.

Blann, K.L., Anderson, J.L., Sands, G.R., Vondracek, B., 2009. Effects of Agricultural Drainage on Aquatic Ecosystems: A Review. Crit. Rev. Environ. Sci. Technol. 39, 909–1001.

Cazorzi, F., Fontana, G.D., Luca, A.D., Sofia, G., Tarolli, P., 2013. Drainage network detection and assessment of network storage capacity in agrarian landscape. Hydrol. Process. 27, 541–553.

Chen, H., Liang, Q., Liang, Z., Liu, Y., Ren, T., 2020. Extraction of connected river networks from multi-temporal remote sensing imagery using a path tracking technique. Remote Sens. Environ. 246.

Choi, S.-S., Cha, S.-H., Tappert, C.C., 2010. A survey of binary similarity and distance measures. J. Systemic, Cybern. Inform. 8, 43–48.

Cira, C.I., Alcarria, R., Manso-Callejo, M.A., Serradilla, F., 2020. A Deep Learning-Based Solution for Large-Scale Extraction of the Secondary Road Network from High-Resolution Aerial Orthoimagery. Appl. Sci.-Basel 10.

Cohen, M.J., Creed, I.F., Alexander, L., Basu, N.B., Calhoun, A.J., Craft, C., D'Amico, E., DeKeyser, E., Fowler, L., Golden, H.E., Jawitz, J.W., Kalla, P., Kirkman, L.K., Lane, C. R., Lang, M., Leibowitz, S.G., Lewis, D.B., Marton, J., McLaughlin, D.L., Mushet, D. M., Raanan-Kiperwas, H., Rains, M.C., Smith, L., Walls, S.C., 2016. Do geographically isolated wetlands influence landscape functions? Proc. Natl. Acad. Sci. USA 113, 1978–1986.

Dollinger, J., Dagès, C., Bailly, J.-S., Lagacherie, P., Voltz, M., 2015. Managing ditches for agroecological engineering of landscape. A Review. Agronomy Sustain. Dev. 35, 999–1020.

Du, L., McCarty, G.W., Zhang, X., Lang, M.W., Vanderhoof, M.K., Li, X., Huang, C., Lee, S., Zou, Z., 2020. Mapping Forested Wetland Inundation in the Delmarva Peninsula, USA Using Deep Convolutional Neural Networks. Remote Sensing 12.

Du, L., McCarty, G.W., Li, X., Rabenhorst, M.C., Wang, Q., Lee, S., Hinson, A.L., Zou, Z., 2021. Spatial extrapolation of topographic models for mapping soil organic carbon using local samples. Geoderma 404.

Elmore, A.J., Julian, J.P., Guinn, S.M., Fitzpatrick, M.C., 2013. Potential stream density in Mid-Atlantic US watersheds. PLoS One 8, e74819.

Fisher, T.R., Benitez, J.A., Lee, K.Y., Sutton, A.J., 2006. History of land cover change and biogeochemical impacts on the Choptank River basin in the mid-Atlantic region of the US. Int. J. Remote Sens. 27, 3683–3703.

Flyckt, J., Andersson, F., Lavesson, N., Nilsson, L., Å gren, A.M., 2022. Detecting ditches using supervised learning on high-resolution digital elevation models. Expert Syst. Appl. 201, 116961.

Fritz, K.M., Hagenbuch, E., D'Amico, E., Reif, M., Wigington, P.J., Leibowitz, S.G., Comeleo, R.L., Ebersole, J.L., Nadeau, T.-L., 2013. Comparing the Extent and Permanence of Headwater Streams From Two Field Surveys to Values From Hydrographic Databases and Maps. JAWRA J. Am. Water Resour. Assoc. 49, 867–882.

Gardner, T.W., Connors, K.F., Hu, H., 2007. Extraction of fluvial networks from SPOT panchromatic data in a low relief, arid basin. Int. J. Remote Sens. 10, 1789–1801.

Hansen, W.F., 2001. Identifying stream types and management implications. For. Ecol. Manage. 143, 39–46.

Heine, R.A., Lant, C.L., Sengupta, R.R., 2008. Development and Comparison of Approaches for Automated Mapping of Stream Channel Networks. Ann. Assoc. Am. Geogr. 94, 477–490.

Herzon, I., Helenius, J., 2008. Agricultural drainage ditches, their biological importance and functioning. Biol. Conserv. 141, 1171–1183.

Hooshyar, M., Kim, S., Wang, D., Medeiros, S.C., 2015. Wet channel network extraction by integrating LiDAR intensity and elevation data. Water Resour. Res. 51, 10029–10046.

Hu, Q., Woldt, W., Neale, C., Zhou, Y.Z., Drahota, J., Varner, D., Bishop, A., LaGrange, T., Zhang, L.G., Tang, Z.H., 2021. Utilizing unsupervised learning, multi-view imaging, and CNN-based attention facilitates cost-effective wetland mapping. Remote Sens. Environ. 267.

Jones, C.N., Evenson, G.R., McLaughlin, D.L., Vanderhoof, M.K., Lang, M.W., McCarty, G.W., Golden, H.E., Lane, C.R., Alexander, L.C., 2018. Estimating restorable wetland water storage at landscape scales. Hydrol. Process. 32, 305–313.

Lang, M.W., Kim, V., McCarty, G.W., Li, X., Yeo, I.-Y., Huang, C., Du, L., 2020. Improved Detection of Inundation below the Forest Canopy using Normalized LiDAR Intensity Data. Remote Sens. (Basel) 12.

Lang, M.W., McCarty, G.W., 2009. Lidar Intensity for Improved Detection of Inundation Below the Forest Canopy. Wetlands 29, 1166–1178.

Lang, M., McCarty, G., Oesterling, R., Yeo, I.-Y., 2012a. Topographic Metrics for Improved Mapping of Forested Wetlands. Wetlands 33, 141–155.

Lang, M., McDonough, O., McCarty, G., Oesterling, R., Wilen, B., 2012b. Enhanced Detection of Wetland-Stream Connectivity Using LiDAR. Wetlands 32, 461–473.

Li, J.Y., Li, T.J., Zhang, L., Sivakumar, B., Fu, X.D., Huang, Y.F., Bai, R., 2020a. A D8-compatible high-efficient channel head recognition method. Environ. Model. Softw. 125.

Li, X., McCarty, G.W., Du, L., Lee, S., 2020b. Use of Topographic Models for Mapping Soil Properties and Processes. Soil Systems 4.

Liaw, A., Wiener, M., 2002. Classification and Regression by randomForest. R News 2, 18–22.

Lindsay, J.B., Dhun, K., 2015. Modelling surface drainage patterns in altered landscapes using LiDAR. Int. J. Geogr. Inf. Sci. 29, 397–411.

Lowrance, R., Altier, L.S., Newbold, J.D., Schnabel, R.R., Groffman, P.M., Denver, J.M., Correll, D.L., Gilliam, J.W., Robinson, J.L., Brinsfield, R.B., Staver, K.W., Lucas, W., Todd, A.H., 1997. Water Quality Functions of Riparian Forest Buffers in Chesapeake Bay Watersheds. Environ Manage 21, 687–712.

Mao, X., Chow, J.K., Su, Z.Y., Wang, Y.H., Li, J.Y., Wu, T., Li, T.J., 2021. Deep learning-enhanced extraction of drainage networks from digital elevation models. Environ. Model. Softw. 144.

McCarty, G.W., McConnell, L.L., Hapeman, C.J., Sadeghi, A., Graff, C., Hively, W.D., Lang, M.W., Fisher, T.R., Jordan, T., Rice, C.P., Codling, E.E., Whitall, D., Lynn, A., Keppler, J., Fogel, M.L., 2008. Water quality and conservation practice effects in the Choptank River watershed. J. Soil Water Conserv. 63, 461–474.

Moore, R.B., Dewald, T.G., 2016. The Road to NHDPlus — Advancements in Digital Stream Networks and Associated Catchments. JAWRA J. Am. Water Resour. Assoc. 52, 890–900.

Moretti, G., Orlandini, S., 2018. Hydrography-Driven Coarsening of Grid Digital Elevation Models. Water Resour. Res. 54, 3654–3672.

Nadeau, T.L., Rains, M.C., 2007. Hydrological connectivity between headwater streams and downstream waters: How science can inform policy. J. Am. Water Resour. Assoc. 43, 118–133.

O'Callaghan, J.F., Mark, D.M., 1984. The extraction of drainage networks from digital elevation data. Computer Vision, Graph., Image Process. 28, 323–344.

O'Neil, G.L., Saby, L., Band, L.E., Goodall, J.L., 2019. Effects of LiDAR DEM Smoothing and Conditioning Techniques on a Topography-Based Wetland Identification Model. Water Resour. Res.

Orlandini, S., Tarolli, P., Moretti, G., Dalla Fontana, G., 2011. On the prediction of channel heads in a complex alpine terrain using gridded elevation data. Water Resour. Res. 47.

Passalacqua, P., Do Trung, T., Foufoula-Georgiou, E., Sapiro, G., Dietrich, W.E., 2010a. A geometric framework for channel network extraction from lidar: Nonlinear diffusion and geodesic paths. J. Geophys. Res. 115.

Passalacqua, P., Tarolli, P., Foufoula-Georgiou, E., 2010b. Testing space-scale methodologies for automatic geomorphic feature extraction from lidar in a complex mountainous landscape. Water Resour. Res. 46.

Passalacqua, P., Belmont, P., Foufoula-Georgiou, E., 2012. Automatic geomorphic feature extraction from lidar in flat and engineered landscapes. Water Resour. Res. 48.

Persendt, F.C., Gomez, C., 2016. Assessment of drainage network extractions in a low-relief area of the Cuvelai Basin (Namibia) from multiple sources: LiDAR, topographic maps, and digital aerial orthophotographs. Geomorphology 260, 32–50.

Pirotti, F., Tarolli, P., 2010. Suitability of LiDAR point density and derived landform curvature maps for channel network extraction. Hydrol. Process. 24, 1187–1197.

Poppenga, S.K., Gesch, D.B., Worstell, B.B., 2013. Hydrography Change Detection: The Usefulness of Surface Channels Derived From LiDAR DEMs for Updating Mapped Hydrography. J. Am. Water Resour. Assoc. 49, 371–389.

Rapinel, S., Hubert-Moy, L., Clement, B., Nabucet, J., Cudennec, C., 2015. Ditch network extraction and hydrogeomorphological characterization using LiDAR-derived DTM in wetlands. Hydrol. Res. 46, 276–290.

Roelens, J., Höfle, B., Dondeyne, S., Van Orshoven, J., Diels, J., 2018a. Drainage ditch extraction from airborne LiDAR point clouds. ISPRS J. Photogramm. Remote Sens. 146, 409–420.

Roelens, J., Rosier, I., Dondeyne, S., Van Orshoven, J., Diels, J., 2018b. Extracting drainage networks and their connectivity using LiDAR data. Hydrol. Process. 32, 1026–1037.

Ronneberger, O., Fischer, P., Brox, T., 2015. U-Net: Convolutional Networks for Biomedical Image Segmentation. Springer International Publishing, Cham, pp. 234–241.

Sangireddy, H., Stark, C.P., Kladzyk, A., Passalacqua, P., 2016. GeoNet: An open source software for the automatic and objective extraction of channel heads, channel network, and channel morphology from high resolution topography data. Environ. Model. Softw. 83, 58–73.

Shedlock, R.J., Denver, J.M., Hayes, M.A., Hamilton, P.A., Koterba, M.T., Bachman, L.J., Phillips, P.J., & Banks, W.S. (1999). Water-quality assessment of the Delmarva Peninsula, Delaware, Maryland, and Virginia; results of investigations, 1987-91. In, *Water Supply Paper*. Reston, Virginia.

Sofia, G., Tarolli, P., Cazorzi, F., Dalla Fontana, G., 2011. An objective approach for feature extraction: distribution analysis and statistical descriptors for scale choice and channel network identification. Hydrol. Earth Syst. Sci. 15, 1387–1402.

Stanislawski, L., Brockmeyer, T., Shavers, E., 2018. Automated road breaching to enhance extraction of natural drainage networks from elevation models through deep learning. Int. Arch. Photogramm. Remote Sens. Spatial Inf. Sci. XLII-4, 597–601.

Stanislawski, L.V., Survila, K., Wendel, J., Liu, Y., Buttenfield, B.P., 2017. An open source high-performance solution to extract surface water drainage networks from diverse terrain conditions. Cartogr. Geogr. Inf. Sci. 45, 319–328.

Stedman, S., & Dahl, T.E. (2008). Status and trends of wetlands in the coastal watersheds of the Eastern United States 1998 to 2004. In: National Oceanic and Atmospheric Administration, National Marine Fisheries Service and U.S. Department of the Interior, Fish and Wildlife Service.

Tarboton, D.G., 1997. A new method for the determination of flow directions and upslope areas in grid digital elevation models. Water Resour. Res. 33, 309–319.

Wu, Q., Lane, C.R., Wang, L., Vanderhoof, M.K., Christensen, J.R., Liu, H., 2018. Efficient Delineation of Nested Depression Hierarchy in Digital Elevation Models for Hydrological Analysis Using Level-Set Method. JAWRA J. Am. Water Resour. Assoc. 55, 354–368.

Wu, J., Liu, H.X., Wang, Z., Ye, L., Li, M., Peng, Y., Zhang, C., Zhou, H.C., 2021. Channel head extraction based on fuzzy unsupervised machine learning method. Geomorphology 391.

Xu, Z.W., Wang, S.W., Stanislawski, L.V., Jiang, Z., Jaroenchai, N., Sainju, A.M., Shavers, E., Usery, E.L., Chen, L., Li, Z.Y., Su, B., 2021. An attention U-Net model for detection of fine-scale hydrologic streamlines. Environ. Model. Softw. 140.

Yang, X.F., Li, X.T., Ye, Y.M., Lau, R.Y.K., Zhang, X.F., Huang, X.H., 2019. Road Detection and Centerline Extraction Via Deep Recurrent Convolutional Neural Network U-Net. IEEE Trans. Geosci. Remote Sens. 57, 7209–7220.

Zhang, X., Han, L., Han, L., Zhu, L., 2020. How Well Do Deep Learning-Based Methods for Land Cover Classification and Object Detection Perform on High Resolution Remote Sensing Imagery. Remote Sens. (Basel) 12.

Zhang, H., Loáiciga, H.A., Feng, L., He, J., Du, Q., 2021. Setting the Flow Accumulation Threshold Based on Environmental and Morphologic Features to Extract River Networks from Digital Elevation Models. ISPRS Int. J. Geo Inf. 10.

Zhu, W., Huang, Y., Zeng, L., Chen, X., Liu, Y., Qian, Z., Du, N., Fan, W., Xie, X., 2019. AnatomyNet: Deep learning for fast and fully automated whole-volume segmentation of head and neck anatomy. Med Phys 46, 576–589.